Self-Assembly of Nanoparticle Amphiphiles with Adaptive Surface Chemistry

Hee-Young Lee, Sun Hae Ra Shin, Aaron M. Drews, Aaron M. Chirsan, Sean A. Lewis, and Kyle J. M. Bishop*

A. Experiment

B. Simulation

A.1. Electrostatic Titration Data (AuNPs)

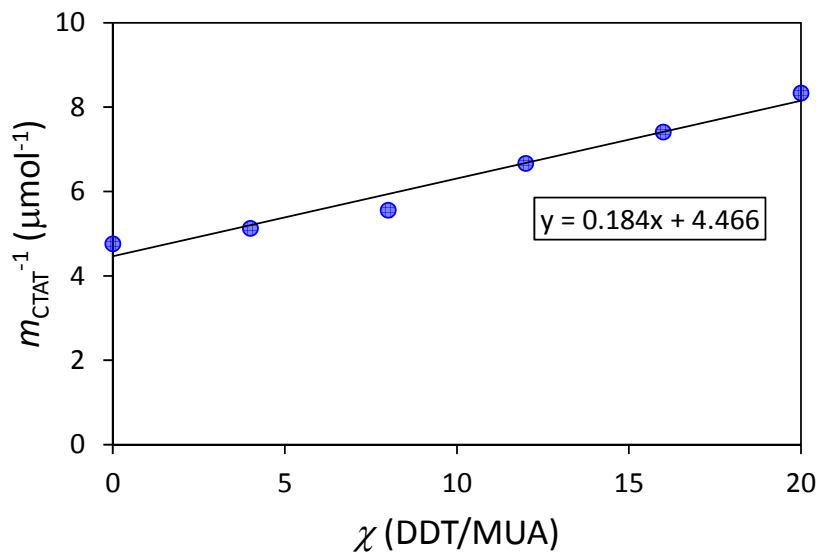**Figure S1.** The plot shows the reciprocal of the precipitation point (moles of CTAT added, m_{CTAT}) as a function of the ligand ratio χ. The line is the best linear fit to the data ($m_{CTAT}^{-1} = a\chi + b$ with $a = 0.18 \pm 0.016$ μmol^{-1} and $b = 4.47 \pm 0.19$ μmol^{-1} where the uncertainties represent standard error). The parameter K relating the ratio of ligands added to that on the surface of the NPs, $\chi_{surf} = K\chi$, is $K = a / b = 0.041 \pm 0.005$.

A.2. Ligand Composition by ^{1}H NMR (AuNPs)

The electrostatic titration method use to quantify the ligand ratio has been validated previously in some detail by Grzybowski *et al.* (see Ref 28; *J. Am. Chem. Soc.* **2007**, 129, 6664) and more recently by Bishop *et al.* (see Ref 22; *J. Am. Chem. Soc.* **2013**, 135, 5950). In these previous works, the results of the electrostatic titrations were validated against the method of Murray *et al.* (see, for example, *J. Am. Chem. Soc.* **1998**, 120, 1906), in which the functionalized NPs were first decomposed via iodine oxidation to quantitatively liberate the ligands as disulfides. The resulting disulfides were then analyzed by ^{1}H NMR.

To further validate the ligand ratios presented in the present work, we repeated the NMR analysis for the amphiphilic NPs with DDT fraction $f = 0.25$ (the chain-forming particles shown in Figure 1b). As a control sample, we first prepared a 3:1 mixture of MUA and DDT ligands (no nanoparticles) in dichloromethane, to which iodine was added to oxidize the thiols to disulfides. After 2 h of sonication, excess iodine was removed by washing with methanol and drying at 65°C to remove the solvent. Subsequently, the disulfide mixtures were dried under vacuum for 12 h to remove traces of water, methanol, and dichloromethane. The resulting disulfides were dissolved in deuterated dichloromethane and analyzed by 300 MHz ^{1}H NMR.

As shown in Figure S2 (a), we confirmed the peaks originating from the methylene group next to the carboxyl group of the MUA thiol (R-C$\boldsymbol{H}_2$-COO-CH$_3$, $\delta \sim 2.28 - 2.33$ ppm) and the methylene group next to the disulfide (C$\boldsymbol{H}_2$-SS, $\delta \sim 2.68 - 2.73$ ppm). The ratio of the integrated peak intensities, $1.42 / 2.00 = 0.71$, gives an estimate of the ligand composition $n^{MUA} / n^{DDT+MUA}$ that agrees to within ~5% of the known value of 0.75. We note that the carboxyl group on MUA reacts with methanol upon heating in the presence of iodine to form the corresponding methyl

ester (K. Ramalinga, P. Vijayalakshmi, T.N.B Kaimal, *Tetrahedron Lett.* **2002**, 43, 879) as evidenced by the singlet at $d \sim 3.65$ ppm (R-CH$_2$-COO-C**H**$_3$).
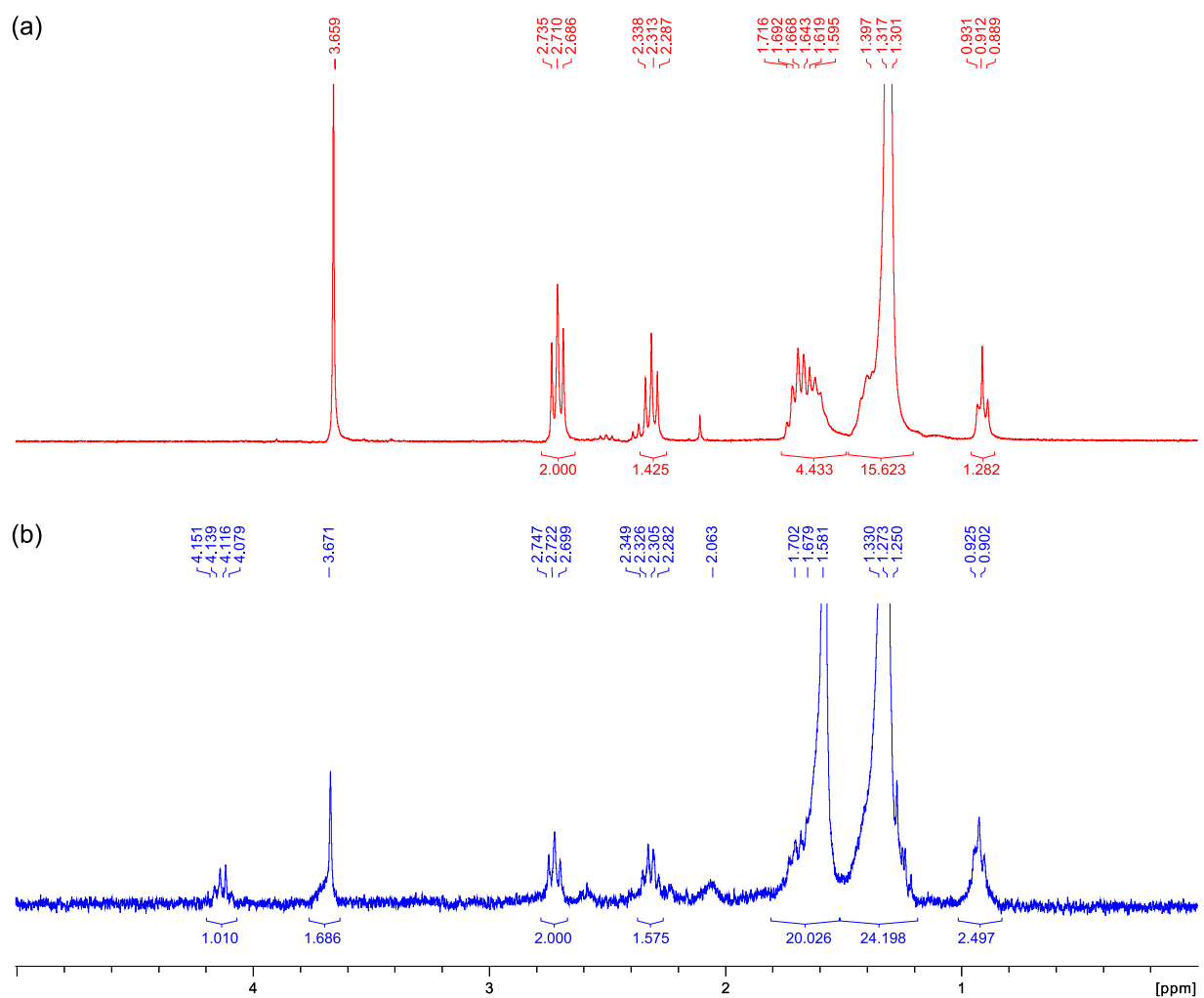

Figure S2. ^{1}H NMR spectra of disulfides formed by of iodine oxidation of MUA and DDT ligands in deuterated dichloromethane. (a) Control sample of 3:1 mixture of MUA and DDT ligands (no nanoparticles). (b) Amphiphilic AuMUA/DDT NPs ($f = 0.25$).

Guided by the control sample, we followed the procedure of Murray *et al.* to quantify the ligand ratio on the surface of the AuMUA/DDT particles. Briefly, AuMUA/DDT NPs dissolved

in water at pH 11 were acidified with HCl to protonate MUA and precipitate the particles from solution. After decanting the supernatant, the precipitated NPs were dissolved in ethanol to which excess of iodine was added. The solution was sonicated for 24 h to fully etch the gold and liberate MUA and DDT ligands as disulfides. As in the control, excess iodine was removed by washing with methanol and drying at 65°C to remove the solvent. Subsequently, the disulfide mixtures were then dried under vacuum for 12 h remove traces of water methanol, and ethanol. The resulting disulfides were dissolved in deuterated dichloromethane, filtered to remove the solid residue of the decomposed NPs, and analyzed by 300 MHz ^{1}H NMR.

The ligand composition was estimated from the integrated peak intensities of the methylene group next to the carboxyl group of the MUA thiol (R-C$\boldsymbol{H_2}$-COO-CH$_2$-CH$_3$ and R-C$\boldsymbol{H_2}$-COO-CH$_3$, $\delta \sim 2.28 - 2.34$ ppm) and methylene group next to the disulfides (C$\boldsymbol{H_2}$SS, $\delta \sim 2.69 - 2.74$ ppm). From the spectrum show in Figure S2 (b), the surface composition is estimated to be n^{MUA} / $n^{DDT+MUA} = 0.78$, which is close to value of 0.75 predicted by electrostatic titrations. Indeed, the ~4% difference between the two methods is comparable to the error seen in the control sample of known composition. As in the control, the carboxyl groups on MUA reacted with both ethanol and methanol to form the corresponding ethyl ester (CH$_2$-COO-C$\boldsymbol{H_2}$-CH$_3$, $\delta \sim 4.11 - 4.13$ ppm) and methyl ester (R-CH$_2$-COO-C$\boldsymbol{H_3}$, $\delta \sim 3.67$ ppm), respectively.

We note that the NMR characterization has several disadvantages as compared to the simpler titration method: (1) it requires large amounts of NPs (*ca.* 10 times that used in titration experiments); and (2) it requires several purification steps that can introduce additional errors. Therefore, in the main text, we quote the results of the electrostatic titration.
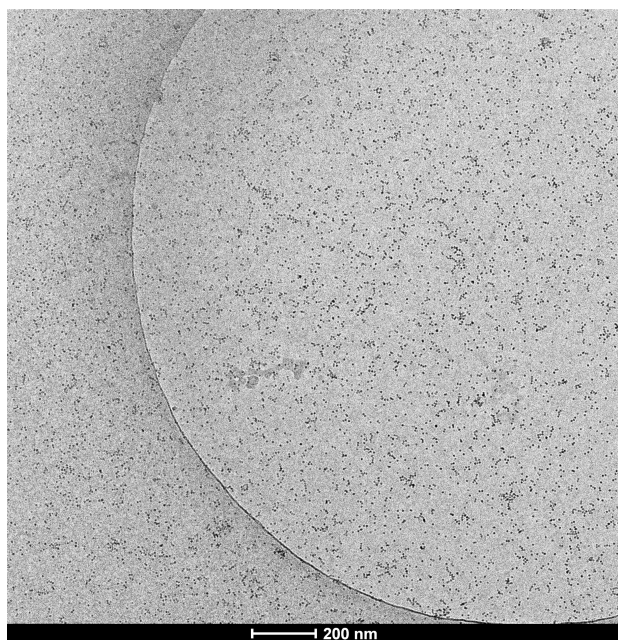
A.3. Cryo-TEM Images (AuNPs)

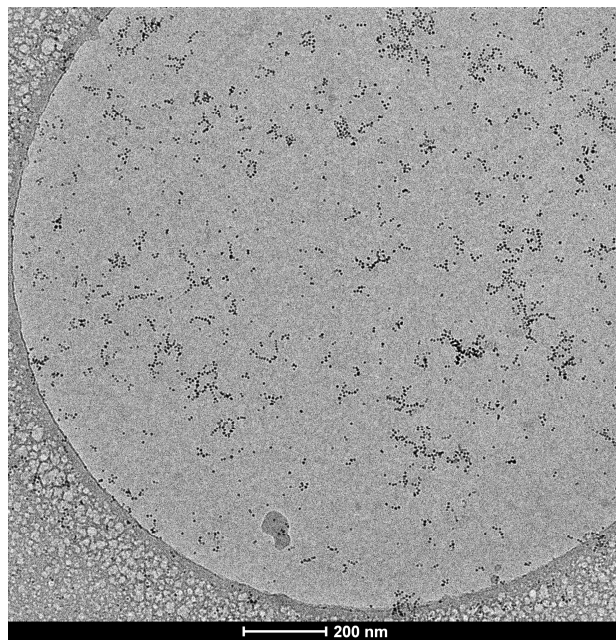The images below correspond to the conditions described in Figure 3 of the main text.
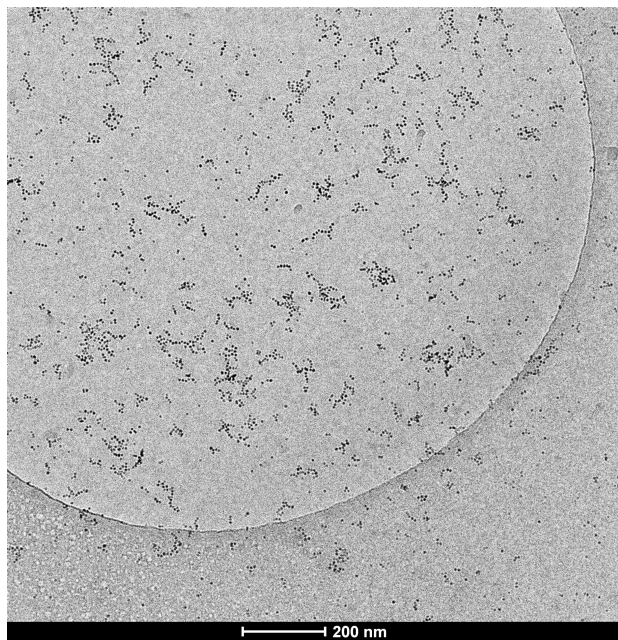
f = **0** (5 mM AuMUA/DDT NPs, 0.2 M TMACl)
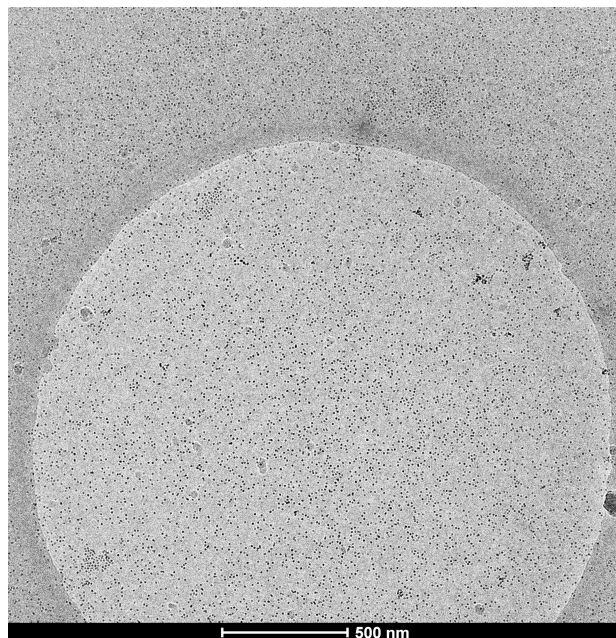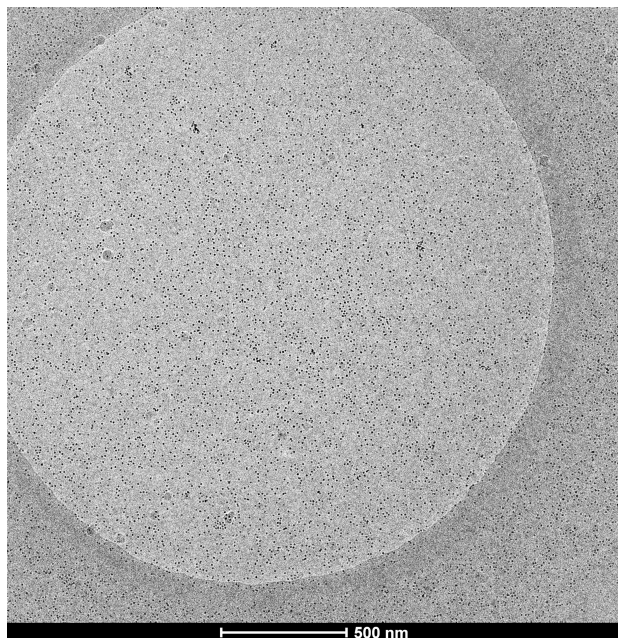
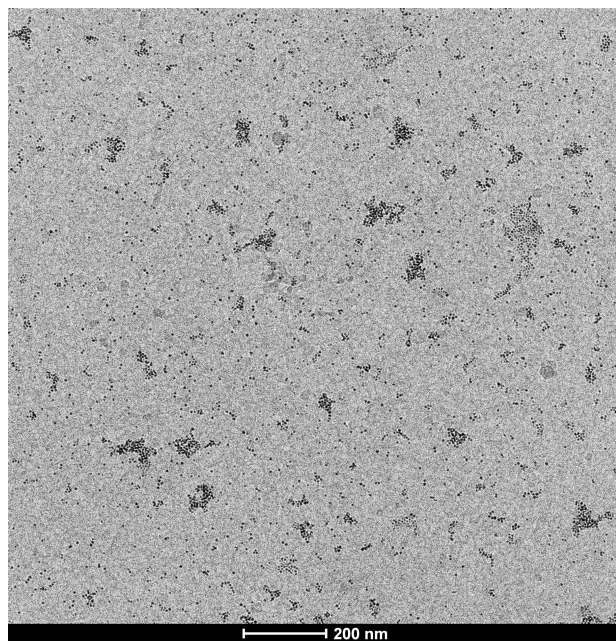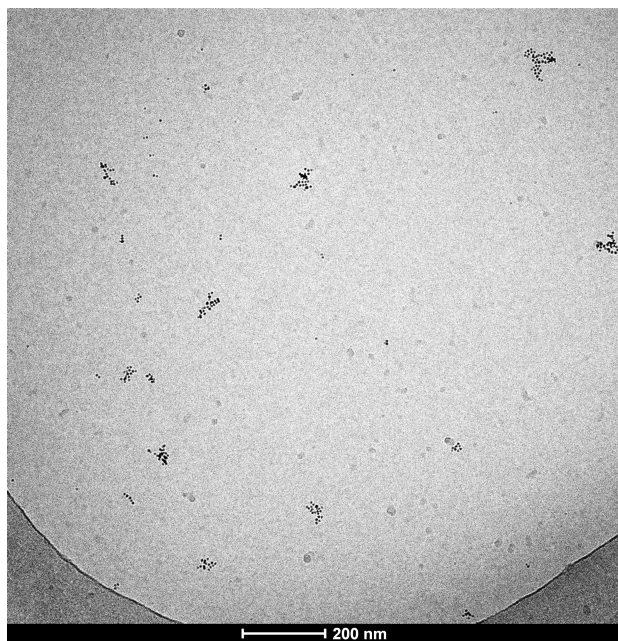*f* = **0.15** (5 mM AuMUA/DDT NPs, 0.2 M TMACl)

***f* = 0.25** (5 mM AuMUA/DDT NPs, 0.2 M TMACl)

***f* = 0.33** (5 mM AuMUA/DDT NPs, 0.2 M TMACl)

Note: The image on the right shows the adsorption of NP clusters on the holey carbon substrate.

A.4. Cryo-TEM Image Analysis

To better quantify the NP structures observed in experiment, we analyzed the cryo-TEM images to estimate the numbers of nearest neighbors for >500 particles for each DDT fraction f (>3000 particles for f = 0, 0.15, and 0.25). Particle centers were located using standard image processing methods (for details, see http://gibbs.engr.ccny.cuny.edu/technical/Tracking/). For each particle, the number of nearest neighbors was defined as the number of particles with separation distance less than 12 nm. This analysis is inherently approximate as it neglects the 3-dimensional structure of the NP clusters; however, it does capture the essential trend – that NP coordination number increases with increasing DDT fraction – which is also evident by visual inspection of the images (see Figure 3 as well as additional images in Section A.3 above). The average number of nearest neighbors (NN) and associated standard deviations are summarized in the table below; these values are quoted in the caption of Figure 3.

DDT Fraction, f	Average NN	Std. Dev. NN
0.00	0.38	0.71
0.15	1.07	1.11
0.25	1.68	1.09
0.33	2.86	1.76

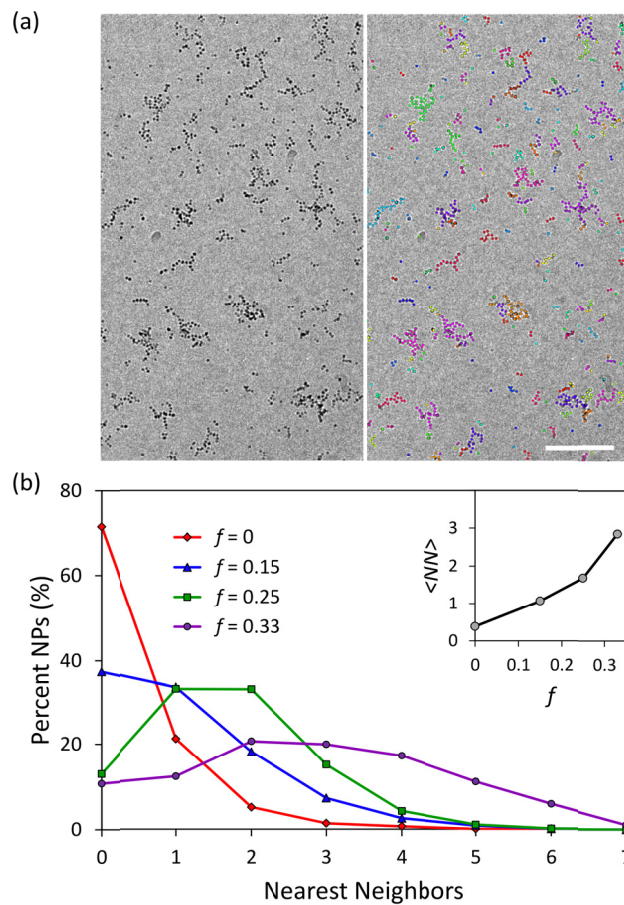**Figure S3.** NP coordination number. **(a)** Cryo-TEM image ($f = 0.25$, $c_s = 0.2$ M) before and after particle identification; different clusters are denoted by different colors. (Scale bar = 200 nm) **(b)** Nearest neighbor distributions for different DDT fractions f as estimated from cryo-TEM images. The inset shows the average number of nearest neighbors as a function of the DDT fraction.
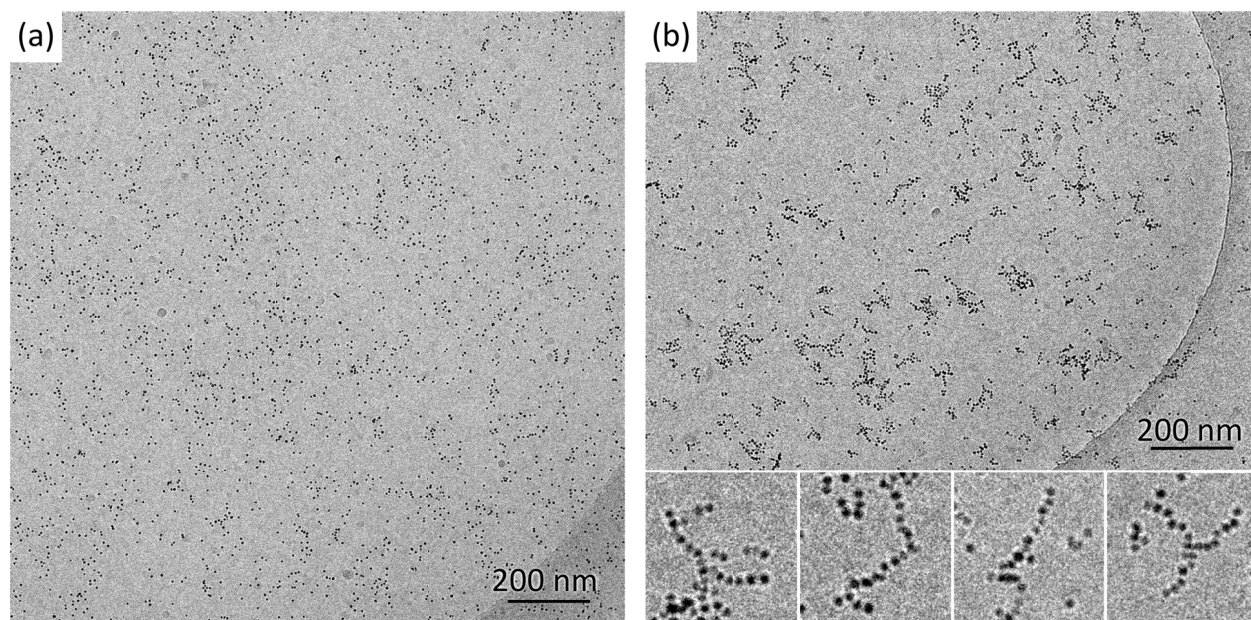
A.5. Effect of Assembly Time

Figure S4. Effect of assembly time. Cryo-TEM images of AuMUA/DDT NPs with DDT coverage $f = 0.25$ from 5 mM NP solutions (on a gold atom basis) containing 0.2 M of TMACl. The image was taken at **(a)** ~1 minute and **(b)** ~ 24 hours after preparing samples.

A.6. Electrostatic Titration Data (CoFe$_2$O$_4$ NPs)
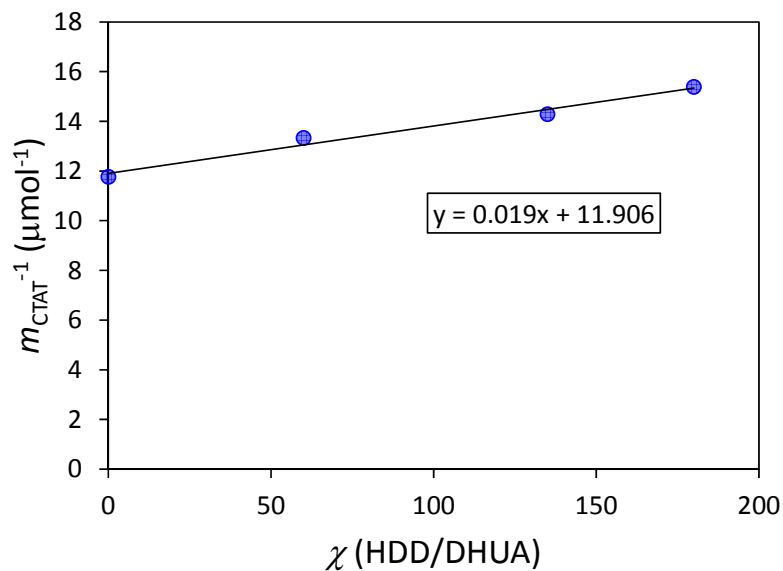
Figure S5. The plot shows the reciprocal of the precipitation point (moles of CTAT added, m_{CTAT}) as a function of the ligand ratio χ. The line is the best linear fit to the data ($m_{CTAT}^{-1} = a\chi + b$ with $a = 0.019 \pm 0.0019$ μmol^{-1} and $b = 11.9 \pm 0.22$ μmol^{-1} where the uncertainties represent standard error). The parameter K relating the ratio of ligands added to that on the surface of the NPs, $\chi_{surf} = K\chi$, is $K = a / b = 0.0016 \pm 0.0002$.

A.7 Cryo-TEM Images (CoFe₂O₄ NPs)

The images below correspond to the conditions described in Figure 5 of the main text.

$f = 0$ (6.66 mg/mL CoFe$_2$O$_4$ NPs, 0.2 M TMACl)
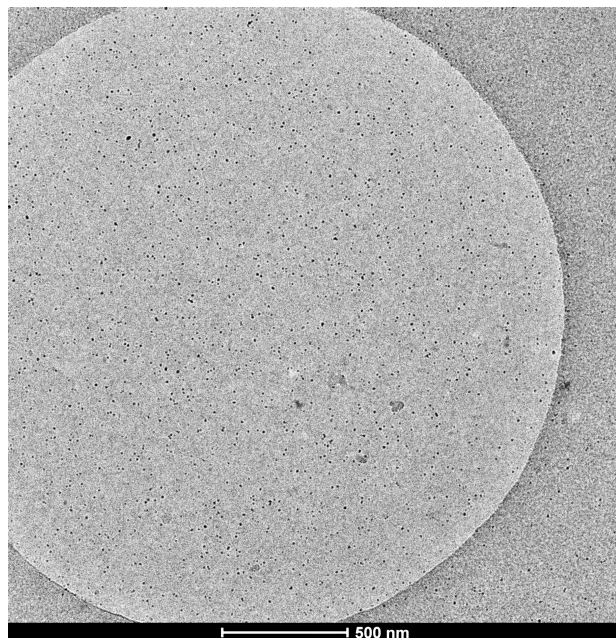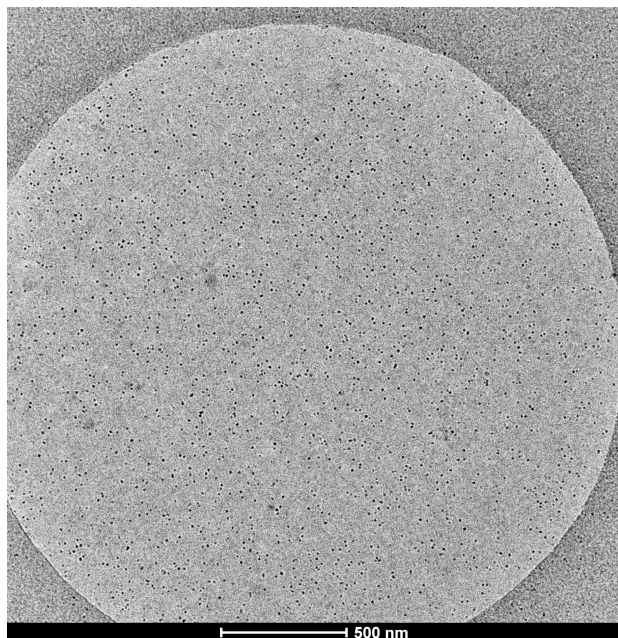
$f = 0.2$ (6.66 mg/mL CoFe$_2$O$_4$ NPs, 0.2 M TMACl)

B.1. Nanoparticle Contacts

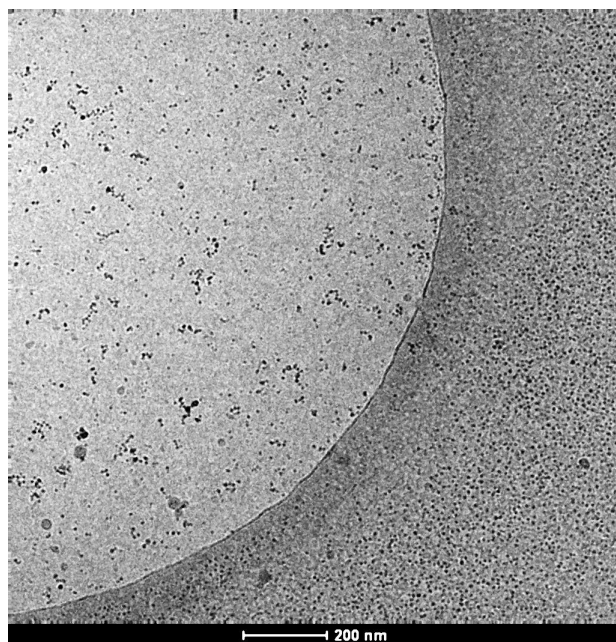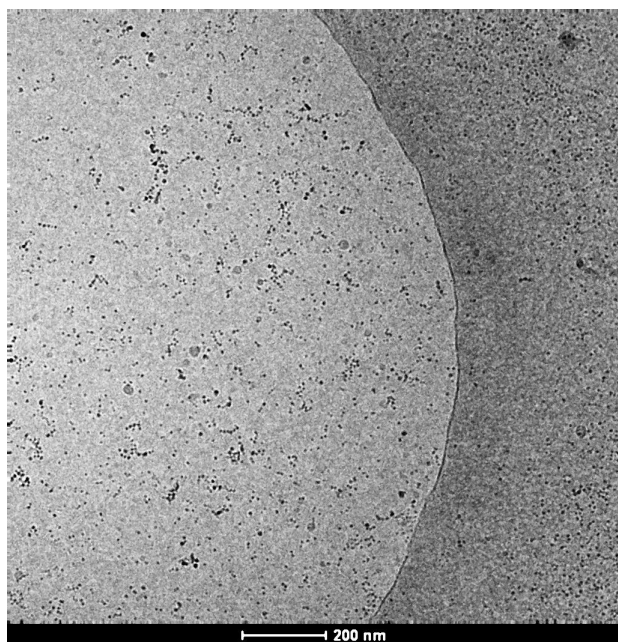The contact between two model NPs is illustrated in Figure S6a. Nanoparticle cores are approximated as perfect spheres of radius $a_c = 3.1$ nm covered with a uniform density of ligands, $\Gamma_L \approx 4.7$ ligands / nm^2 ($N_L \approx 560$ ligands per NP) [Leff, D. V.; Ohara, P. C.; Heath, J. R.; Gelbart, W. M. *J. Phys. Chem.* **1995**, 99, 7036-7041]. Given the ligand length of $\delta \approx 2$ nm, we define an outer radius $a_o = a_c + \delta = 5.1$ nm, which characterizes the range of hydrophobic interactions; NPs separated by more than $2a_o$ do not interact. At contact, the distance between two NPs is assumed to be $d = 2a_i = 7.4$ nm, which corresponds to a circular contact region of radius $r = 3.5$ nm. The interparticle distance d was chosen as to accommodate the volume of ligands V_L within the contact region (assuming a ligand density, $\rho_L \approx 0.85$ g/mL).

To estimate the maximum number of ligands that contribute to an NP-NP contact, we assume that H_{max} is proportional to the solid angle Ω of the contact region. For the two particle geometry detailed above, this assumption implies that

$$\Omega = 2\pi\left(1 - \frac{a_i}{a_o}\right) \approx 1.71, \tag{S1}$$

$$H_{max} = \frac{\Omega}{4\pi}N_L \approx 0.136 N_L, \tag{S2}$$

where N_L is the total number of ligands on a single NP. Importantly, when more than two NPs interact with one another, their contact regions can overlap thereby reducing the solid angle of each interaction. In the cubic-close-packed (ccp) lattice used in the MC simulations, each NP-NP bond is flanked by four lattice sites; the solid angle of the interactions depends on the presence / absence of particles within these neighboring sites as illustrated in Figure S6b. In the

simulations, the maximum number of ligands within a contact region H_{max} was computed using equation (S2) with solid angles determined by the geometry of the contact.

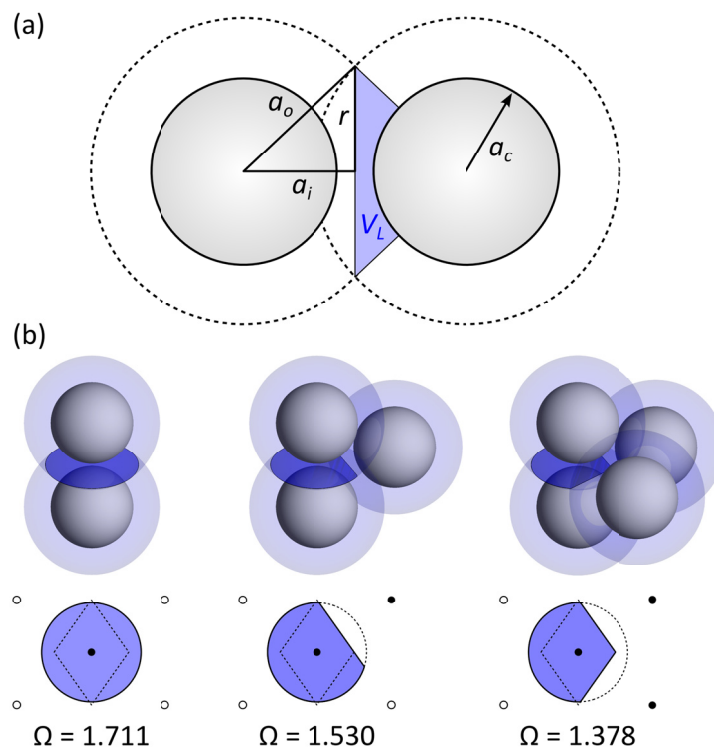**Figure S6. (a)** Schematic illustration of two NPs in contact highlighting the relevant quantities described in the text. **(b)** The contact area between two NPs is characterized by the solid angle Ω and depends on the presence of neighboring particles (open or closed circles). Three of the 2^4 possible configurations are illustrated here; solid angles for other configurations can be derived from these values.

B.2. Electrostatic Interactions

In the model presented in the main text, electrostatic interactions are characterized by a pairwise interaction energy ε_{es} between nearest neighbors. Here, we use the nonlinear Poisson Boltzmann equation to (i) solve for the electric potential in and around two NPs at contact and (ii) compute the interaction energy under the experimental conditions.
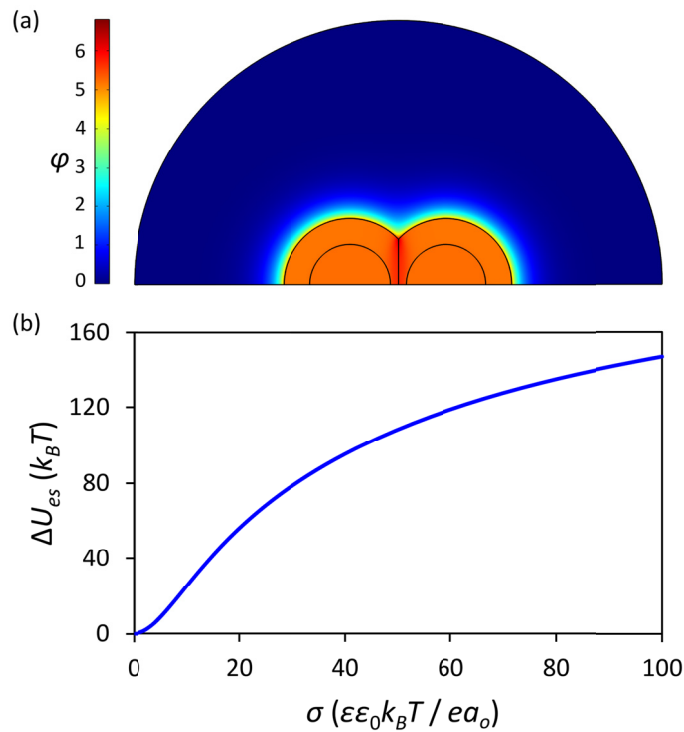
Figure S7. **(a)** Computed electrostatic potential φ (scaled by $k_B T / e$) in and around two NPs in contact. Here, the screening parameter is $\kappa a_o = 3.02$ [$\kappa^{-1} = (\varepsilon \varepsilon_0 k_B T / 2 n_o e^2)^{1/2}$ is the screening length], charge density is $\sigma e a_o / \varepsilon \varepsilon_0 k_B T = 50$, and the dielectric constant of the ligands is $\varepsilon_L / \varepsilon = 0.025$. **(b)** Electrostatic interaction energy between two spheres in contact as a function of charge density σ (on the free particles) for the conditions described in (a).

Electric Potential. The electric potential φ surrounding the NPs is assumed to obey the Poisson-Boltzmann (PB) equation,

$$\nabla^2 \varphi = \frac{2en_0}{\varepsilon\varepsilon_0} \sinh\left(\frac{e\varphi}{k_B T}\right),$$
(S3)

where e is the elementary charge, n_0 is the (monovalent) salt concentration, ε is the dielectric constant of the solvent, ε_0 is the vacuum permittivity, and $k_B T$ is the thermal energy. The interior of the particle is modeled as a conductive sphere of radius a_c surrounded by a dielectric medium corresponding to the ligands (dielectric constant, $\varepsilon_L \approx 2$). The potential φ_L within the ligand shell is governed by the Laplace equation

$$\nabla^2 \varphi_L = 0 .$$
(S4)

Together, equations (S3) and (S4) govern the potential in and around the two particles subject to the following boundary conditions: (1) Far from the particles, the potential is zero, $\varphi(\infty) = 0$. (2) At the surface of each particle, the potential is continuous ($\varphi = \varphi_L$), and the surface charge is related to the potential as

$$\varepsilon_0 (\varepsilon_L \nabla \varphi_L - \varepsilon \nabla \varphi) \cdot \mathbf{n} = \sigma ,$$
(S5)

where $\mathbf{n}$ is the vector normal to the surface, and σ is the constant surface charge density. Importantly, when two NPs come into contact, we assume that none of the charged groups remain within the contact area due to the strong energetic penalty of moving a charge from a high dielectric environment (the aqueous electrolyte) to a low dielectric environment (the hydrophobic ligands). (3) At the surface of the NP cores, the potential is constant, and the net charge on the core is zero. With these preliminaries, equations (S3) and (S4) can be solved

numerically using a commercial finite element solver (COMSOL) to determine the electric potential in and around the two particles (Figure S7a).

Electrostatic Energy. For constant surface charge σ, the electrostatic energy is expressed as

$$U_{es} = \int_S \int_0^\sigma \varphi(\mathbf{x}, \sigma') d\sigma' dS , \qquad (S6)$$

where the first integral describes the charging of the particle surface S from zero to σ, and the second is carried out over that surface. The electrostatic interaction energy is given by

$$\Delta U_{es} = U_{es}^{(2)} - 2U_{es}^{(1)} , \qquad (S7)$$

where $U_{es}^{(1)}$ is the electrostatic energy of a free particle with charge density σ, and $U_{es}^{(2)}$ is the electrostatic energy of the two particles in contact (Figure S7a) with charge density $\frac{1}{2}(3 - a_i / a_o)\sigma$, which corresponds to the same total charge distributed over a smaller area. Figure S6b plots this interaction as a function of surface charge for the experimental conditions.

Assuming a hydrophobic ligand coverage of $f = 0.14$ (corresponding to one hydrophobic patch), the dimensionless charge density (on the free particles) is estimated to be $\sigma e a_o / \varepsilon \varepsilon_0 k_B T \approx 67$, which corresponds to an interaction energy of $\Delta U_{es} \approx 120 k_B T$.

B.3. Monte Carlo Exchange Moves

To simulate the dilute clusters described in the main text, we developed an efficient type of Monte Carlo move that allows for the direct exchange of particles between two clusters, thereby accelerating their equilibration. Here, we describe the implementation of this move and show that it satisfies the detailed balance condition.

Exchange Move Implementation

1) Pick one of the N_p particles at random.

2) With probability p, move it to one of the N_s lattice sites chosen at random. Alternatively, with probability $(1 - p)$, move it to one of the $z_{max} = 12$ sites adjacent to another randomly selected particle.

3) Accept the move with probability,

$$acc(o \rightarrow n) = \min\left[1, \frac{1 + \kappa z(o)}{1 + \kappa z(n)} \exp\left(-\beta[U(n) - U(o)]\right)\right],$$
(S8)

where $z(o)$ is the number of nearest neighbors of the particle in the "old" configuration, and $z(n)$ is the number of nearest neighbors of the particle in the "new" configuration, $U(o)$ and $U(n)$ refer to the energies of the "old" and "new" configurations, $\beta = 1/k_B T$ is the inverse temperature, and κ is a tunable parameter, which is related to the probability p as

$$\kappa \equiv \frac{N_s(1-p)}{z_{max} N_p p}.$$
(S9)

We now show that the algorithm outlined above satisfies the detailed balance condition:

$$\mathcal{N}(o) \times \alpha(o \rightarrow n) \times acc(o \rightarrow n) = \mathcal{N}(n) \times \alpha(n \rightarrow o) \times acc(n \rightarrow o),$$
(S10)

where $\mathcal{N}(o)$ is the equilibrium probability of being in configuration o, $\alpha(o \rightarrow n)$ is the probability of generating configuration n from configuration o, and $acc(n \rightarrow o)$ is the probability of accepting this move. The equilibrium distribution is simply the Boltzmann distribution

$$\mathcal{N}(o) = \frac{1}{Z} \exp\left(-\beta U(o)\right), \tag{S11}$$

where Z is the partition function. The probability $\alpha(o \rightarrow n)$ is given by

$$\alpha(o \rightarrow n) = \left(\frac{1}{N_p}\right)\left(\frac{p}{N_s} + \frac{(1-p)z(n)}{N_p z_{max}}\right), \tag{S12}$$

where the two terms in correspond to steps 1 and 2 above. To ensure detailed balance, the ratio of the acceptance probabilities must obey

$$\frac{acc(o \rightarrow n)}{acc(n \rightarrow o)} = \frac{\mathcal{N}(n)\alpha(n \rightarrow o)}{\mathcal{N}(o)\alpha(o \rightarrow n)}. \tag{S13}$$

Substituting equations (S11) and (S12), this ratio becomes

$$\frac{acc(o \rightarrow n)}{acc(n \rightarrow o)} = \frac{1 + \kappa z(o)}{1 + \kappa z(n)} \exp\left(-\beta[U(n) - U(o)]\right), \tag{S14}$$

which is satisfied by equation (S8).

To determine a suitable value for the probability p (or equivalently κ), we consider the scenario in which a free particle forms one bond of energy $-\varepsilon$ with another particle. The rate of this process is

$$K(o \rightarrow n) = \mathcal{N}(o) \times \alpha(o \rightarrow n) \times acc(o \rightarrow n), \tag{S15}$$

$$K(o \rightarrow n) \propto \frac{1 + \kappa}{1 + \kappa(z_{max} N_p / N_s)} \min\left[1, \frac{1}{1 + \kappa} \exp\left(\beta\varepsilon\right)\right]. \tag{S16}$$

Assuming the system is dilute ($z_{max} N_p / N_s \ll 1$), this rate is maximal when

$$\kappa_{max} = \exp(\beta\varepsilon) - 1. \qquad\qquad (S17)$$

For smaller values ($\kappa \ll \kappa_{max}$), the probability of attempting such a move becomes increasingly low; for larger values ($\kappa \gg \kappa_{max}$), the acceptance probability becomes the limiting factor. We used the estimate (S17) in all simulations.
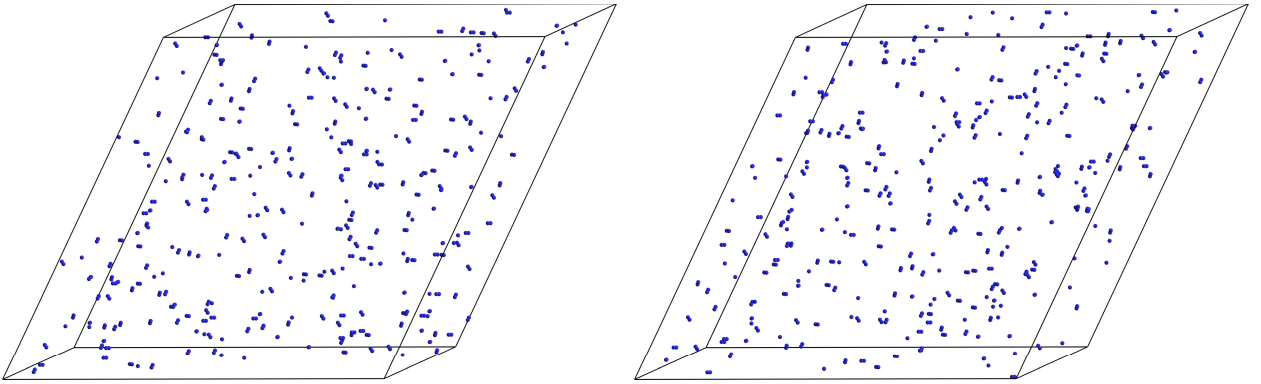
B.4. Additional Simulation Images

The images below correspond to the conditions described in Figure 4c of the main text – namely, $\rho = 2 \times 10^{-4}$, $\beta = 100$, and $\alpha = 90$ with the valence parameter v listed below.
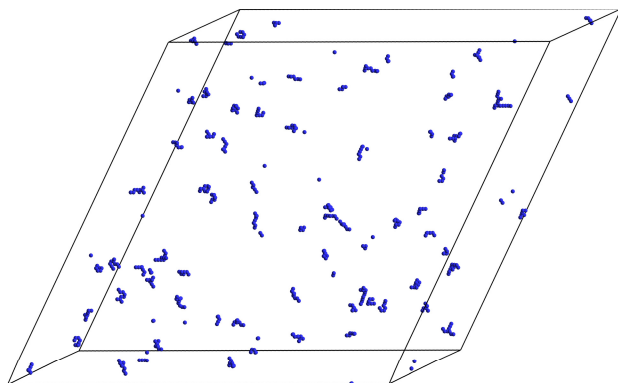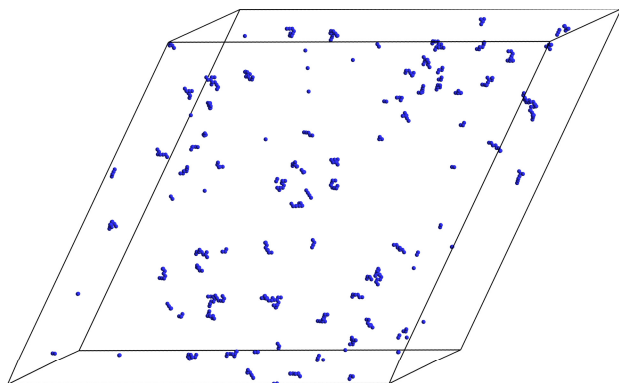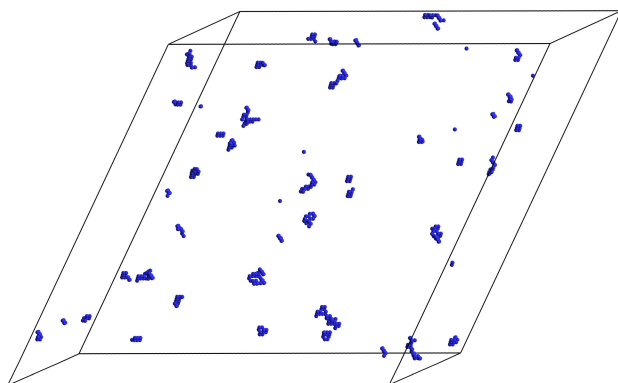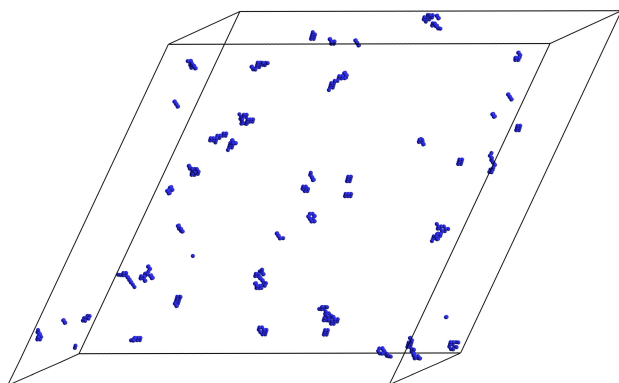
$v = 0$

$v = 1.2$

ν = 1.8
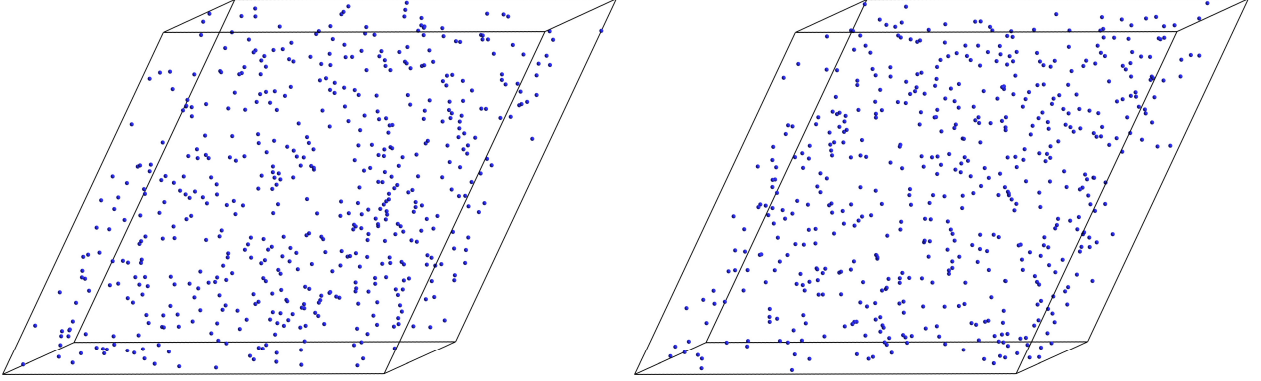
ν = 2.4

B.5. "Control" Simulations without Adaptive Surface Chemistry

Extended chain-like clusters do not form from particles with isotropic interactions between nearest neighbors. This is illustrated below in Figure S8 which shows typical equilibrium configurations for two different, pairwise interaction strengths (scaled by the thermal energy k_BT). Weak interactions ($\alpha < 2.5$) lead to a disordered, gas-like state; strong interactions ($\alpha > 2.5$) lead to phase separation and the formation of a dense crystalline phase. Finite size clusters can be found at intermediate interaction strengths; however, no chain-like clusters were observed.
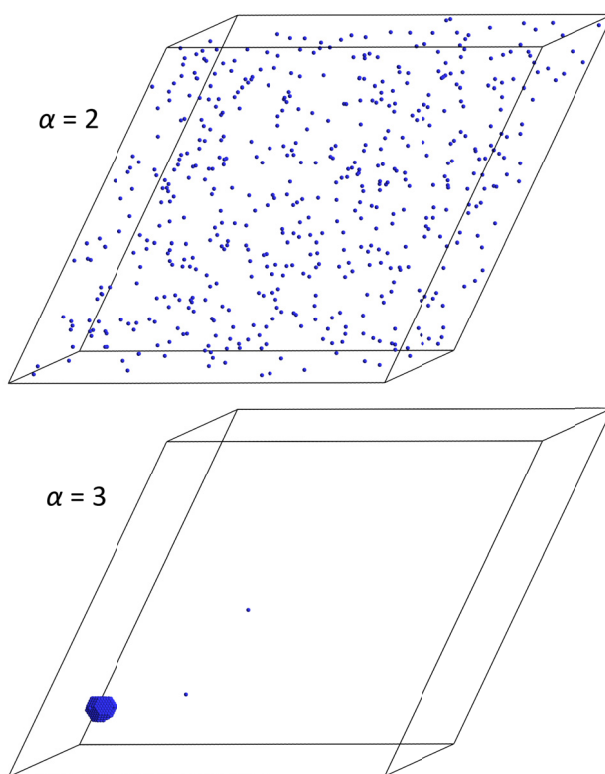

Figure S8. Particle configurations obtained by Monte Carlo simulations of 549 particles on a ccp lattice ($140\times140\times140$) with attractive interactions between nearest neighbors; α is the pairwise interaction energy scaled by k_BT. These snap shots were obtained after equilibration of the system over the course of 5×10^6 attempted MC exchange moves.

B.6. Improving Chain Monodispersity

In experiments and simulations, the distribution of chain lengths was polydisperse. The MC simulations can offer insights into narrowing the chain length distributions. In particular, for the coordination parameter $1 < v < 2$, MC simulations give more monodisperse NP chains when $\beta - \alpha \sim \alpha \gg 1$ (Figure S9). Under these conditions, the electrostatic penalty for additional bonds beyond that needed to shield the hydrophobic ligands is large relative to the thermal energy, $\alpha \gg 1$. At the same time, there is also a strong penalty for clusters that do not shield all of their hydrophobic ligands from the aqueous surroundings, $\beta - \alpha \gg 1$. Together, these conditions drive the formation of minimal energy clusters that shield all hydrophobic ligands using the fewest possible NP-NP interactions; for $1 < v < 2$, these minimal energy clusters are often (though not exclusively) particle chains (see Figure S9a). Physically, these conditions imply the need to strengthen the hydrophobic attraction (e.g., by changing the length of the hydrophobic ligands on the particles' surface) or reduce the electrostatic repulsion.
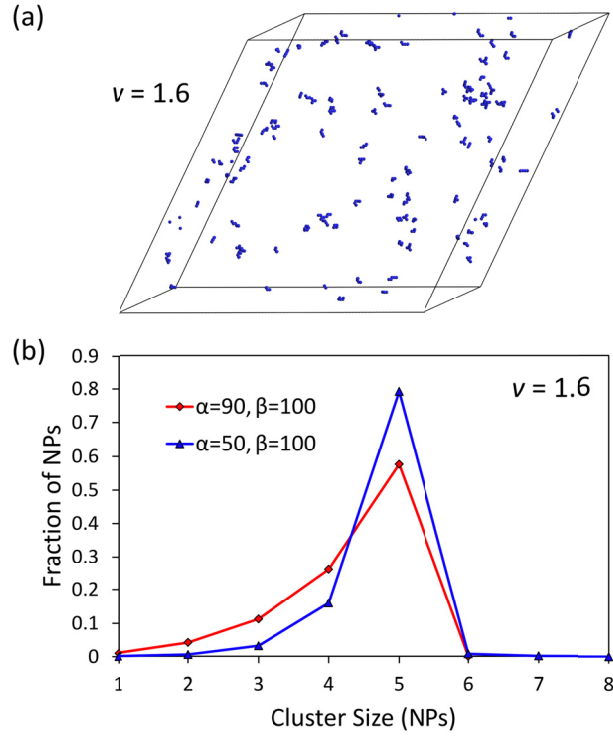
(a)

$v = 1.6$

(b)

Figure S9. Increasing the effective attraction between NPs (i.e., increasing $\beta - \alpha$ from 10 to 50) acts to narrow the cluster size distribution, which is centered on particle chains of length $N = 2 / (2 - v) = 5$. **(a)** Equilibrium particle configuration for $v = 1.6$, $\alpha = 50$, and $\beta = 100$. **(b)** Cluster size distribution for two different values of α. When hydrophobic interactions are stronger (relative to electrostatic repulsion), the size distribution is more narrow.